# A Bayesian Nonparametrics View into Deep Representations

## Supplementary material

### A Collapsed Gibbs Sampling for DP-GMM

We estimate posterior distributions over DP-GMM parameters using Collapsed Gibbs Sampling (CGS) algorithm [Neal, 2000]. Here we describe CGS in more details. The derivation below closely follows the one from [Murphy, 2012, chapters 24.2.4 & 25.2.4].

CGS steps consist of iterative sampling of component indicators $c_i$ for observations $\boldsymbol{x}_i \in \mathcal{D}$, $i = 1, \ldots, N$. During this sampling, CGS maintains a set of $K$ components, where $K$ itself is a random variable (components can be added or removed). Each component $k \in \{1, \ldots, K\}$ is described by a set $\boldsymbol{\theta}_k$ of parameters of the Normal-inverse-Wishart posterior distribution over its mean $\boldsymbol{\mu}_k$ and covariance $\boldsymbol{\Sigma}_k$:

$$p(\boldsymbol{\mu}_k, \boldsymbol{\Sigma}_k \mid \mathcal{D}) = p(\boldsymbol{\mu}_k, \boldsymbol{\Sigma}_k \mid \boldsymbol{\theta}_k) = NIW(\boldsymbol{\mu}_k, \boldsymbol{\Sigma}_k \mid \boldsymbol{\theta}_k), \quad \boldsymbol{\theta}_k = \{\boldsymbol{m}_k, \nu_k, \kappa_k, \boldsymbol{S}_k\}. \tag{1}$$

Given a vector of current component assignments $\boldsymbol{c} = \{c_1, \ldots, c_N\}$, CGS samples a new assignment for $\boldsymbol{x}_i$ from the conditional $p(c_i \mid \boldsymbol{c_{-i}}, \boldsymbol{x_i}, \alpha, \boldsymbol{\theta})$:

$$p(c_i = k \mid \boldsymbol{c}_{-i}, \boldsymbol{x}_i, \alpha, \boldsymbol{\theta}) \propto p(c_i = k \mid \boldsymbol{c}_{-i}, \alpha) p(\boldsymbol{x}_i \mid \boldsymbol{x}_{-i}, c_i = k, \boldsymbol{c}_{-i}, \boldsymbol{\theta}). \tag{2}$$

Here $\boldsymbol{c}_{-i}$, $\boldsymbol{x}_{-i}$ stand for, respectively, component assignments and the dataset with the $i$-th element removed; $\boldsymbol{\theta}$ is the collection of all component parameters. The first term in the above product comes from the Chinese-Restaurant Process (CRP), and has the form:

$$p(c_i = k \mid \boldsymbol{c}_{-i}, \alpha) = \begin{cases} \frac{N_{k,-i}}{\alpha+N-1} & \text{if } k \text{ already exists,} \\ \frac{\alpha}{\alpha+N-1} & \text{if } k \text{ is a new component.} \end{cases} \tag{3}$$

The second term can be derived by noticing that given the component assignment ($c_i = k$), observation $\boldsymbol{x}_i$ becomes conditionally independent from observations assigned to other components:

$$p(\boldsymbol{x}_i \mid \boldsymbol{x}_{-i}, c_i = k, \boldsymbol{c}_{-i}, \boldsymbol{\theta}) = p(\boldsymbol{x}_i \mid \boldsymbol{x}_{-i,k}, \boldsymbol{\theta}_k), \tag{4}$$

where $\boldsymbol{x}_{-i,k}$ are observations assigned to the $k$-th component, except $\boldsymbol{x}_i$. The above term has a closed-form solution computed by integrating out $\boldsymbol{\mu}_k$, $\boldsymbol{\Sigma}_k$ parameters, namely a multivariate Student's t-distribution (more details are given in appendix B):

$$p(\boldsymbol{x}_i \mid \boldsymbol{x}_{-i,k}, \boldsymbol{\theta}_k) = p(\boldsymbol{x}_i \mid \boldsymbol{\theta}_k) = \int p(\boldsymbol{x}_i \mid \boldsymbol{\mu}_k, \boldsymbol{\Sigma}_k) p(\boldsymbol{\mu}_k, \boldsymbol{\Sigma}_k \mid \boldsymbol{\theta}_k) d\boldsymbol{\mu}_k d\boldsymbol{\Sigma}_k. \tag{5}$$

When $k$ is a new (empty) component, the above density reduces to the Student's t-distribution with parameters derived from the NIW prior hyper-parameters, i.e. from $\boldsymbol{\theta}_0 = \{\boldsymbol{m}_0, \nu_0, \kappa_0, \boldsymbol{S}_0\}$:

$$p(\boldsymbol{x}_i \mid \boldsymbol{\theta}_0) = \int p(\boldsymbol{x}_i \mid \boldsymbol{\mu}_k, \boldsymbol{\Sigma}_k) p(\boldsymbol{\mu}_k, \boldsymbol{\Sigma}_k \mid \boldsymbol{\theta}_0). \tag{6}$$

Note also that the density from which we are sampling component assignments $p(c_i \mid \boldsymbol{c}_{-i}, \boldsymbol{x}_i, \alpha, \boldsymbol{\theta})$ is a categorical distribution over $c_i$. After sampling from it, one has to update the parameters of the NIW posterior of the newly sampled component (to account for the new member $\boldsymbol{x}_i$). Further, before calculating any quantities necessary to compute $p(c_i \mid \boldsymbol{c}_{-i}, \boldsymbol{x}_i, \alpha, \boldsymbol{\theta})$ (e.g. predictive densities for $\boldsymbol{x}_i$), observation $\boldsymbol{x}_i$ must be removed from the old component, reflecting the conditioning on $\boldsymbol{x}_{-i,k}$.

The probability distribution for component assignments (Eqn. 2) depends on $\alpha$, i.e. the concentration parameter in the Dirichlet Process prior. We do not assume a fixed value for $\alpha$, but explicitly account for its uncertainty by treating it as a model parameter. To this end, we put a $Gamma(1,1)$ prior on $\alpha$. Under this prior the conditional $p(\alpha \mid K, N)$ – which is required by CGS – admits a simple sampling [Escobar and West, 1995].

We choose the values of hyper-parameters $\boldsymbol{\theta}_0$ in a way that puts a weakly-informative, data-dependent prior on component means and covariances. Specifically, we follow guidelines in [Fraley and Raftery, 2007], and set the $\boldsymbol{\theta}_0$ values to:

$$\begin{gathered} \boldsymbol{m}_0 = \frac{1}{N}\sum_{i=1}^{N}\boldsymbol{x}_i, \quad \boldsymbol{S}_0 = \frac{\operatorname{diag}(\boldsymbol{S}_{\overline{x}})}{K_0^{2/D}}, \\ \nu_0 = D+2, \quad \kappa_0 = 0.01, \end{gathered} \tag{7}$$

where $D$ is the data dimensionality, and:

$$K_0 = \alpha \log\left(1+\frac{N}{\alpha}\right), \quad \boldsymbol{S}_{\overline{x}} = \frac{1}{N}\sum_{i=1}^{N}\left(\boldsymbol{x}_i - \boldsymbol{m}_0\right)\left(\boldsymbol{x}_i - \boldsymbol{m}_0\right)^T. \tag{8}$$

Here, $K_0$ is the prior expectation for the number of components and $\boldsymbol{S}_{\overline{x}}$ is the empirical covariance.

## B DP-GMM posterior predictive distribution

Here we derive the formula for the Posterior Predictive distribution given component assignments: $p(\boldsymbol{x}^* \mid \mathcal{D}, \boldsymbol{c})$. The output from CGS is a Markov chain, where at each step we have component assignments $\boldsymbol{c} = \{c_i\}_{i=1}^N$ and posterior distributions $p(\boldsymbol{\mu}_k, \boldsymbol{\Sigma}_k \mid \mathcal{D})$ over component parameters $\{\boldsymbol{\mu}_k, \boldsymbol{\Sigma}_k\}_{k=1}^K$. Because of the conjugate NIW prior choice for means and covariances, the posterior is also a NIW distribution:

$$p(\boldsymbol{\mu}_k, \boldsymbol{\Sigma}_k) = NIW(\boldsymbol{\mu}_k, \boldsymbol{\Sigma}_k \mid \mathbf{m}_k, \nu_k, \kappa_k, \boldsymbol{S}_k). \tag{9}$$

The posterior predictive over a new observation $\boldsymbol{x}^*$ given the dataset $\mathcal{D}$ and component assignments $\boldsymbol{c}$ can be written as:

$$\begin{aligned} p(\boldsymbol{x}^* \mid \mathcal{D}, \boldsymbol{c}) &= \int p(\boldsymbol{x}^* \mid \boldsymbol{\theta}, \boldsymbol{c}) p(\boldsymbol{\theta} \mid \mathcal{D}, \boldsymbol{c}) d\boldsymbol{\theta} \\ &= \int \left[\sum_{k=1}^{K} p(\boldsymbol{x}^* \mid \boldsymbol{\theta}_k) p(c^* = k \mid \boldsymbol{c})\right] p(\boldsymbol{\theta} \mid \mathcal{D}, \boldsymbol{c}) d\boldsymbol{\theta}. \end{aligned} \tag{10}$$

Posterior over component parameters expands to:

$$p(\boldsymbol{\theta} \mid \mathcal{D}, \boldsymbol{c}) = p\left(\{\boldsymbol{\mu}_k, \boldsymbol{\Sigma}_k\}_{k=1}^K \mid \mathcal{D}, \boldsymbol{c}\right) = \prod_{k=1}^{K} p(\boldsymbol{\mu}_k, \boldsymbol{\Sigma}_k \mid \mathcal{D}_k). \tag{11}$$

Above, we leverage the fact that given component assignments the posterior over joint set of parameters factorizes over components; $\mathcal{D}_k$ denotes observations assigned to the $k$-th component, i.e $\mathcal{D}_k = \{\boldsymbol{x}_i : c_i = k\}$. From the model definition it is clear that:

$$p(\boldsymbol{x}^* \mid c^* = k) = p(\boldsymbol{x}^* \mid \boldsymbol{\mu}_k, \boldsymbol{\Sigma}_k). \tag{12}$$

Now, let $\alpha_k = p(c^* = k \mid \boldsymbol{c})$ be the predictive mixture weights. By plugging Eqns. 11 and 12 into Eqn. 10 we obtain:

$$\begin{aligned} &\int \left[\sum_{k=1}^{K} \alpha_k p(\boldsymbol{x}^* \mid \boldsymbol{\mu}_k, \boldsymbol{\Sigma}_k)\right] \prod_{j=1}^{K} p(\boldsymbol{\mu}_j, \boldsymbol{\Sigma}_j \mid \mathcal{D}_j) d\boldsymbol{\mu} d\boldsymbol{\Sigma} \\ &= \sum_{k=1}^{K} \int \alpha_k p(\boldsymbol{x}^* \mid \boldsymbol{\mu}_k, \boldsymbol{\Sigma}_k) \prod_{j=1}^{K} p(\boldsymbol{\mu}_j, \boldsymbol{\Sigma}_j \mid \mathcal{D}_j) d\boldsymbol{\mu} d\boldsymbol{\Sigma} \\ &= \sum_{k=1}^{K} \int \left[\int \alpha_k p(\boldsymbol{x}^* \mid \boldsymbol{\mu}_k, \boldsymbol{\Sigma}_k) p(\boldsymbol{\mu}_k, \boldsymbol{\Sigma}_k \mid \mathcal{D}_k) d\boldsymbol{\mu}_k d\boldsymbol{\Sigma}_k\right] \prod_{j \neq k} p(\boldsymbol{\mu}_j, \boldsymbol{\Sigma}_j \mid \mathcal{D}_j) d\boldsymbol{\mu}_{-k} d\boldsymbol{\Sigma}_{-k} \\ &= \sum_{k=1}^{K} \alpha_k \int p(\boldsymbol{x}^* \mid \boldsymbol{\mu}_k, \boldsymbol{\Sigma}_k) p(\boldsymbol{\mu}_k, \boldsymbol{\Sigma}_k \mid \mathcal{D}_k) d\boldsymbol{\mu}_k d\boldsymbol{\Sigma}_k, \end{aligned} \tag{13}$$

where $\boldsymbol{\mu}_{-k}$ and $\boldsymbol{\Sigma}_{-k}$ are jointly means and covariances of components other than the $k$-th one. Expression under the last integral in Eqn. 13 is tractable, thanks to the conjugacy of the Normal-inverse-Wishart prior to the Gaussian likelihood. Specifically, it is the probability density function of a multivariate Student's t-distribution Murphy [2012, 2007]:

$$\begin{aligned}&\int \mathcal{N}(\boldsymbol{x}^* \mid \boldsymbol{\mu}_k, \boldsymbol{\Sigma}_k) NIW(\boldsymbol{\mu}_k, \boldsymbol{\Sigma}_k \mid \boldsymbol{m_k}, \nu_k, \kappa_k, \boldsymbol{S}_k) d\boldsymbol{\mu}_k d\boldsymbol{\Sigma}_k \\ &= St\left(\boldsymbol{x}^* \mid \boldsymbol{m}_k, \frac{\kappa_k + 1}{\kappa_k(\nu_k - D + 1)}\boldsymbol{S}_k, \nu_k - D + 1\right).\end{aligned} \tag{14}$$

Finally, posterior predictive density (10) can be written as a mixture of multivariate Student's t-distributions with weights $\{\alpha_{k=1}^K\}$:

$$p(\boldsymbol{x}^* \mid \mathcal{D}, \boldsymbol{c}) = \sum_{k=1}^{K} \alpha_k St\left(\boldsymbol{x}^* \mid \boldsymbol{m}_k, \beta_k \boldsymbol{S}_k, \nu_k - D + 1\right), \quad \beta_k = \frac{\kappa_k + 1}{\kappa_k(\nu_k - D + 1)}. \tag{15}$$

The only thing left is to derive the predictive mixture weights: $\{\alpha_{k=1}^K\}$. Recall that $\alpha_k$ is the probability of choosing the $k$-th component for a new observation given the existing component assignments $\boldsymbol{c}$. The set of predictive weights $\{\alpha_{k=1}^K\}$ therefore forms a categorical distribution $p(c^* \mid \boldsymbol{c})$ over the components. It can be calculated by marginalizing out the Dirichlet distributed component weights:

$$\begin{aligned}\alpha_k = p(c^* = k \mid \boldsymbol{c}) &= \int p(c^* = k \mid \boldsymbol{\pi}) p(\boldsymbol{\pi} \mid \boldsymbol{c}) d\boldsymbol{\pi} \\ &= \int \mathrm{Cat}(c^* = k \mid \boldsymbol{\pi}) \mathrm{Dir}(\boldsymbol{\pi} \mid \boldsymbol{c}) d\boldsymbol{\pi} = \frac{N_k + \alpha_0}{N(1 + \alpha_0)},\end{aligned} \tag{16}$$

where $\alpha_0$ is the concentration parameter in the Dirichlet Process prior and $N_k$ is the number of observations assigned to the $k$-th component. Note that predictive mixture weights depend only on the concentration parameter and the number of observations assigned to each component.

## C CNN experiment details and additional results

**Datasets and image augmentation.** CNN experiments (Section 4) were run on CIFAR-10 [Krizhevsky, 2009] and Mini-ImageNet [Vinyals et al., 2016] datasets. To adapt Mini-ImageNet to a typical image classification task, we concatenated the provided training, validation and test subsets (without support and evaluation splits in training data) and then randomly split the dataset into $50,000$ training and $10,000$ test examples. Finally, we resized the images to $42 \times 42$ pixels. CIFAR experiments used the standard train/test split. Image augmentation was implemented as a random $32 \times 32$ (CIFAR) or $42 \times 42$ (Mini-ImageNet) pixel crop from an input with 4 (CIFAR) or 5 (Mini-ImageNet) pixel padding, followed by a random horizontal flip.

**Network architectures and training hyper-parameters.** CNN architectures used in experiments are summarized in Table C.1. All networks were trained for 60 epochs using stochastic gradient descent with learning rate $\epsilon = 0.01$, momentum $\mu = 0.9$ (with Nesterov accelerated gradient), $L_2$ penalty $\lambda = 10^{-6}$ and a batch size equal to 512 examples. Networks with additional regularization had 20% dropout after each nonlinearity.

**Additional results.** Results for architectures not included in Section 4 are summarized in Fig. C.1. These results give further support to conclusions from main CNN experiments: a) memorizing networks learn more complex representations than networks trained on true labels, b) unlike image augmentation, dropout significantly increases representational complexity in CNNs; this effect diminishes with network width, and c) absent image augmentation, deep but narrow nets exhibit increased representational complexity in middle layers.

## D VAE experiment details and additional results

**Datasets.** VAE experiments were carried out on CelebA [Liu et al., 2015] and Anime [Ani] datasets. CelebA examples were prepared by taking a $150 \times 150$ central crop and resizing it to $64 \times 64$ pixels. Anime images were resized to $96 \times 96$ pixels. Both datasets were randomly split into train/test subsets: 150000/52599 split for CelebA and 50000/13632 split for Anime images.

| CNN 11x512 | CNN 11x384 | CNN 11x256 | CNN 11x192 | CNN 11x128 |
|---|---|---|---|---|
| conv. $3 \times 3$ $c = 64$ | conv. $3 \times 3$ $c = 48$ | conv. $3 \times 3$ $c = 32$ | conv. $3 \times 3$ $c = 24$ | conv. $3 \times 3$ $c = 16$ |
| same | | | | |
| conv. $3 \times 3$ $c = 128$, $s = 2$ | conv. $3 \times 3$ $c = 96$, $s = 2$ | conv. $3 \times 3$ $c = 64$, $s = 2$ | conv. $3 \times 3$ $c = 48$, $s = 2$ | conv. $3 \times 3$ $c = 32$, $s = 2$ |
| conv. $3 \times 3$ $c = 128$ | conv. $3 \times 3$ $c = 96$ | conv. $3 \times 3$ $c = 64$ | conv. $3 \times 3$ $c = 48$ | conv. $3 \times 3$ $c = 32$ |
| same | | | | |
| conv. $3 \times 3$ $c = 256$, $s = 2$ | conv. $3 \times 3$ $c = 192$, $s = 2$ | conv. $3 \times 3$ $c = 128$, $s = 2$ | conv. $3 \times 3$ $c = 96$, $s = 2$ | conv. $3 \times 3$ $c = 64$, $s = 2$ |
| conv. $3 \times 3$ $c = 256$ | conv. $3 \times 3$ $c = 192$ | conv. $3 \times 3$ $c = 128$ | conv. $3 \times 3$ $c = 96$ | conv. $3 \times 3$ $c = 64$ |
| same | | | | |
| conv. $3 \times 3$ $c = 512$, $s = 2$ | conv. $3 \times 3$ $c = 384$, $s = 2$ | conv. $3 \times 3$ $c = 256$, $s = 2$ | conv. $3 \times 3$ $c = 192$, $s = 2$ | conv. $3 \times 3$ $c = 128$, $s = 2$ |
| conv. $3 \times 3$ $c = 512$ | conv. $3 \times 3$ $c = 384$ | conv. $3 \times 3$ $c = 256$ | conv. $3 \times 3$ $c = 192$ | conv. $3 \times 3$ $c = 128$ |
| CIFAR: same; Mini-ImageNet: same with $s = 2$ | | | | |
| Fully Connected (logits) | | | | |

| CNN 8x256 | CNN 8x192 | CNN 8x128 |
|---|---|---|
| conv. $3 \times 3$ $c = 64$ | conv. $3 \times 3$ $c = 48$ | conv. $3 \times 3$ $c = 32$ |
| same | | |
| conv. $3 \times 3$ $c = 128$, $s = 2$ | conv. $3 \times 3$ $c = 96$, $s = 2$ | conv. $3 \times 3$ $c = 64$, $s = 2$ |
| conv. $3 \times 3$ $c = 128$ | conv. $3 \times 3$ $c = 96$ | conv. $3 \times 3$ $c = 64$ |
| same | | |
| conv. $3 \times 3$ $c = 256$, $s = 2$ | conv. $3 \times 3$ $c = 192$, $s = 2$ | conv. $3 \times 3$ $c = 128$, $s = 2$ |
| conv. $3 \times 3$ $c = 256$ | conv. $3 \times 3$ $c = 192$ | conv. $3 \times 3$ $c = 128$ |
| CIFAR: same; Mini-ImageNet: same with $s = 2$ | | |
| Fully Connected (logits) | | |

Table C.1: CNN architectures used in experiments (Section 4). Each convolutional layer is followed by batch normalization and ReLU nonlinearity. Dropout – when used – is applied after ReLU. All conv layers use 1 pixel zero-padding. $c$ - number of output channels; $s$ - layer stride (default 1).

**Model architectures and training details.** Architectures for encoder and decoder networks follow closely those used by Tolstikhin et al. [2018] and are summarized in the table D.2. All models had a latent space with $d = 64$ dimensions. Training was carried out for 60 epochs using Adam optimizer [Kingma and Ba, 2015] with a constant learning rate: $\epsilon = 0.001$ and a batch size equal to 64 images. We trained standard $\beta$-VAE models with $\beta \in \{0.01, 0.1, 1.0, 4.0, 10.0, 30.0, 50.0\}$ and MMD-VAE models with $\beta \in \{1.0, 4.0, 30.0, 50.0, 100.0, 200.0, 500.0, 1000.0\}$.

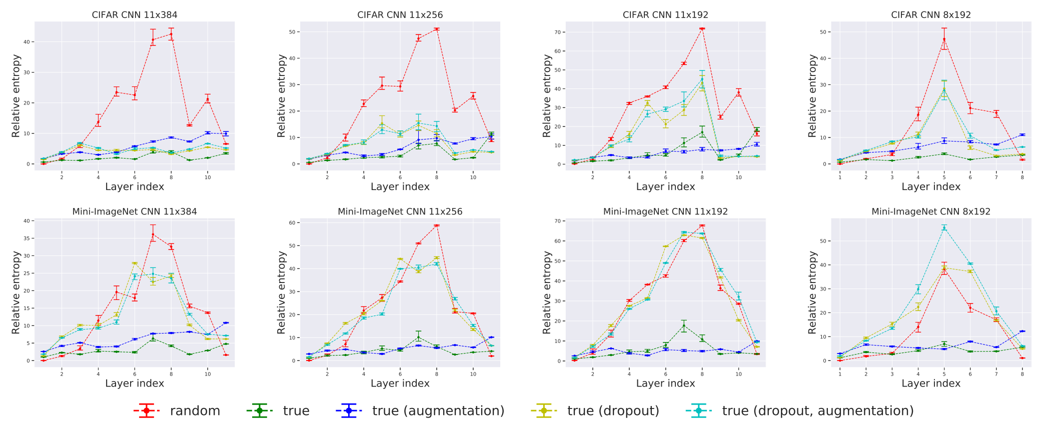

Figure C.1: Relative entropies of posterior predictive distributions for CNN representations. Results for CNN architectures not included in Section 4.

| **Encoder** | **Decoder** |
|---|---|
| conv. $5 \times 5$, $c = 128$, $s = 2$ | Fully Connected: $8 \cdot 8 \cdot 1024$ (Celeb) or $12 \cdot 12 \cdot 1024$ (Anime) |
| conv. $5 \times 5$, $c = 256$, $s = 2$ | FS conv. $5 \times 5$, $c = 512$, $s = 2$ |
| conv. $5 \times 5$, $c = 512$, $s = 2$ | FS conv. $5 \times 5$, $c = 256$, $s = 2$ |
| conv. $5 \times 5$, $c = 1024$, $s = 2$ | FS conv. $5 \times 5$, $c = 128$, $s = 2$ |
| Fully Connected: $64 \cdot 2$ | FS conv. $5 \times 5$, $c = 3$, $s = 1$ |

Table D.2: Convolutional encoder and decoder architectures used in VAE experiments. FS conv. – fractionally strided convolution; $c$ – number of output channels, $s$ – stride. Each convolution and fractionally strided convolution is followed by a batch normalization and ReLU nonlinearity.

**Component counts in CGS traces.** Our primary tools for judging complexity of aggregated posteriors in VAE models are relative entropy and total correlation between dimensions in posterior predictive (Section 3). That said, findings from Section 5 are further supported by distributions of component counts in CGS traces, pictured in Fig. D.2. In standard $\beta$-VAEs, increasing regularization strength simplifies the set of inferred latent codes to the point where it can be explained (by DP-GMM) using just one component. In MMD-VAEs regularization has no obvious influence on the number of components in CGS traces. Note, however, that these results should be interpreted with care – specifically, they do not speak to the number of components in the data generating distribution. Indeed, Dirichlet Process is not consistent for the number of components [Miller and Harrison, 2013, 2014]. Rather, results in Fig. D.2 can be seen as the number of components (from an infinite mixture) observed in a finite set of available data points.

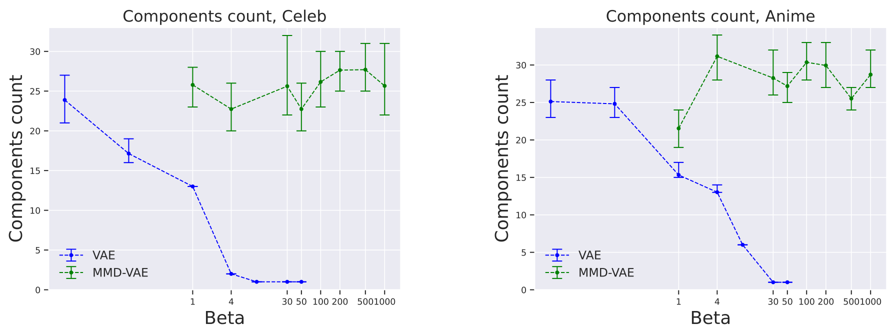

Figure D.2: Component counts in CGS traces for standard $\beta$-VAEs and MMD-VAEs. In each case we report mean, minimum and maximum component count across sampled CGS steps.

**Additional samples.** Figures D.3 and D.4 present additional image samples generated with latent codes drawn from a posterior predictive density $p(\boldsymbol{z}^* \mid \boldsymbol{c})$.

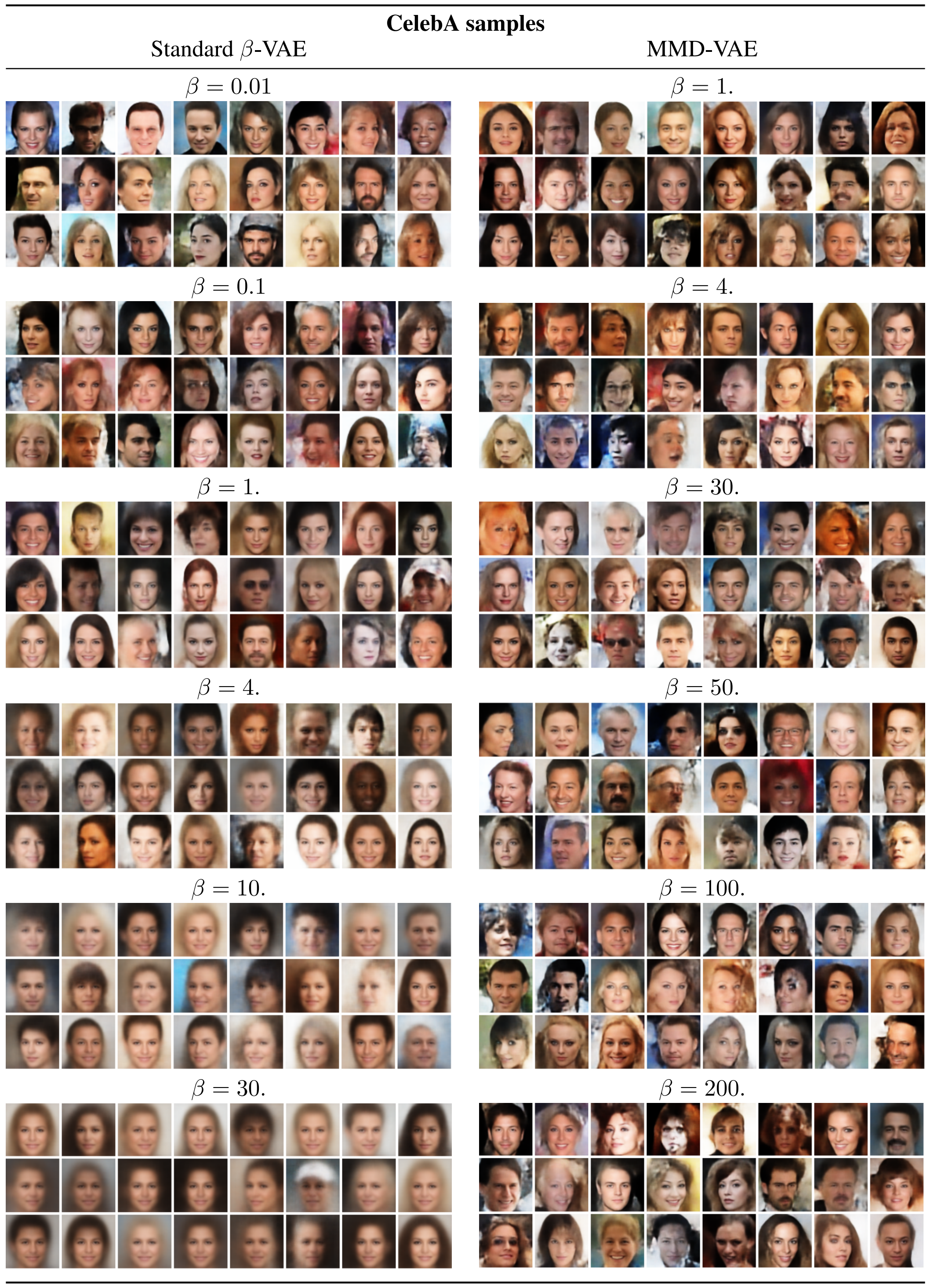

Figure D.3: CelebA samples generated with latent codes drawn from a posterior predictive density.

| **Anime samples** | |
|---|---|
| Standard $\beta$-VAE | MMD-VAE |
| $\beta = 0.01$ 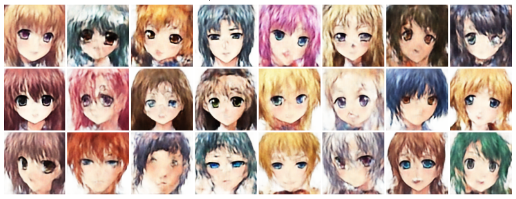 | $\beta = 1.$ 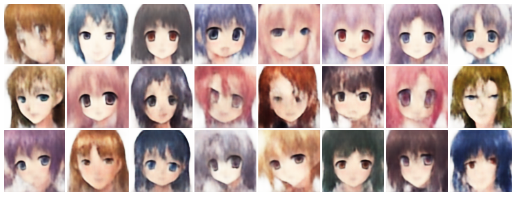 |
| $\beta = 0.1$ 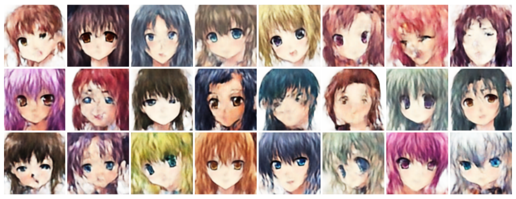 | $\beta = 4.$ 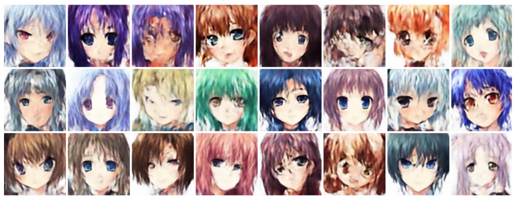 |
| $\beta = 1.$ 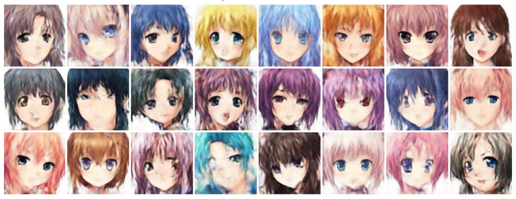 | $\beta = 30.$ 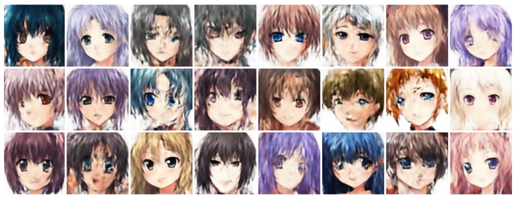 |
| $\beta = 4.$ 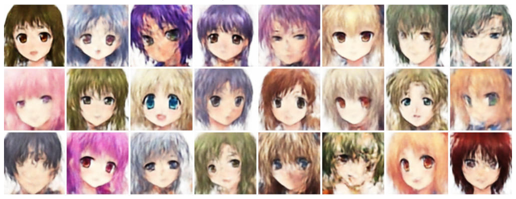 | $\beta = 50.$ 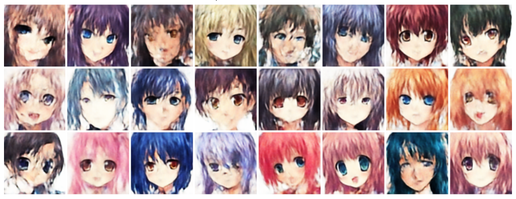 |
| $\beta = 10.$ 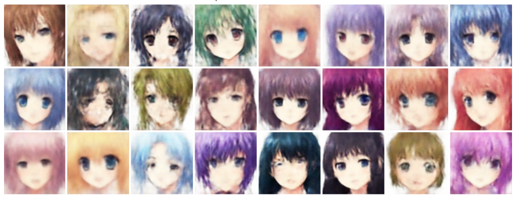 | $\beta = 100.$ 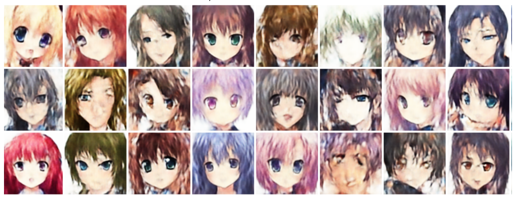 |
| $\beta = 30.$ 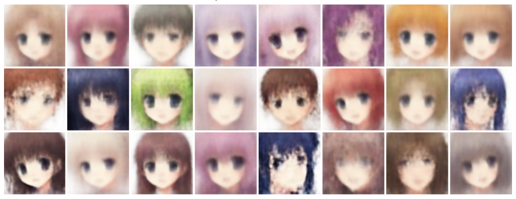 | $\beta = 200.$ 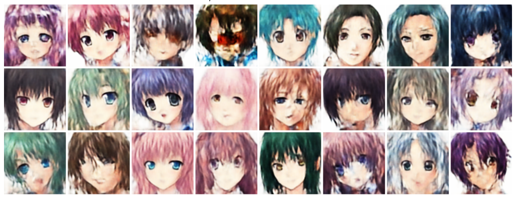 |

Figure D.4: Anime samples generated with latent codes drawn from a posterior predictive density.

## References

A collection of high-quality anime faces. `https://github.com/Mckinsey666/Anime-Face-Dataset`. Accessed: 2020-05-01.

Michael D Escobar and Mike West. Bayesian density estimation and inference using mixtures. *Journal of the American Statistical Association*, 90(430):577–588, 1995.

Chris Fraley and Adrian E. Raftery. Bayesian regularization for normal mixture estimation and model-based clustering. *J. Classification*, 24(2):155–181, 2007.

Diederik P. Kingma and Jimmy Ba. Adam: A method for stochastic optimization. In *3rd International Conference on Learning Representations, ICLR 2015, San Diego, CA, USA, May 7-9, 2015, Conference Track Proceedings*, 2015.

Alex Krizhevsky. Learning multiple layers of features from tiny images. Technical report, 2009.

Ziwei Liu, Ping Luo, Xiaogang Wang, and Xiaoou Tang. Deep learning face attributes in the wild. In *2015 IEEE International Conference on Computer Vision, ICCV 2015, Santiago, Chile, December 7-13, 2015*, pages 3730–3738. IEEE Computer Society, 2015.

Jeffrey W. Miller and Matthew T. Harrison. A simple example of dirichlet process mixture inconsistency for the number of components. In *Advances in Neural Information Processing Systems 26: 27th Annual Conference on Neural Information Processing Systems 2013. Proceedings of a meeting held December 5-8, 2013, Lake Tahoe, Nevada, United States*, pages 199–206, 2013.

Jeffrey W. Miller and Matthew T. Harrison. Inconsistency of pitman-yor process mixtures for the number of components. *Journal of Machine Learning Research*, 15(96):3333–3370, 2014.

Kevin P. Murphy. Conjugate bayesian analysis of the gaussian distribution. Technical report, 2007.

Kevin P. Murphy. *Machine learning - a probabilistic perspective*. Adaptive computation and machine learning series. MIT Press, 2012.

Radford M Neal. Markov chain sampling methods for dirichlet process mixture models. *Journal of computational and graphical statistics*, 9(2):249–265, 2000.

Ilya O. Tolstikhin, Olivier Bousquet, Sylvain Gelly, and Bernhard Schölkopf. Wasserstein auto-encoders. In *6th International Conference on Learning Representations, ICLR 2018, Vancouver, BC, Canada, April 30 - May 3, 2018, Conference Track Proceedings*, 2018.

Oriol Vinyals, Charles Blundell, Tim Lillicrap, Koray Kavukcuoglu, and Daan Wierstra. Matching networks for one shot learning. In *Advances in Neural Information Processing Systems 29: Annual Conference on Neural Information Processing Systems 2016, December 5-10 2016, Barcelona, Spain*, pages 3630–3638, 2016.